Overview of steady state tokamak plasma experiments on TRIAM-1M

H. Zushi 1), S. Itoh 1), K. Hanada 1), K. Nakamura 4), M. Sakamoto 1), E. Jotaki 1), M. Hasegawa 4), Y. D. Pan *2*), S. V. Kulkarni 3), A. Iyomasa 1), S. Kawasaki 1), H. Nakashima 1), N. Yoshida 1,4), K Tokunaga 4), T. Fujiwara 4), M. Miyamoto *5*), H. Nakano 5), M. Yuno 5), A. Murakami 5), S. Nakamura 5), N. Sakamoto 5), K. Shinoda 5), S. Yamazoe 5), H. Akanishi 5), K. Kuramoto 5), Y. Matsuo 5), A Iwamae *6*), T Fuijimoto *6*), A Komori 7), T Morisaki 7), H Suzuki *7*), S Masuzaki *7*), Y Hirooka *7*), Y Nakashima 8), O Mitarai 9)

Advanced Fusion Research Center, Research Institute for Applied Mechanics, Kyushu University, Kasuga 816-8580, Fukuoka, Japan[1)],
Southwestern Institute of Physics China [2)],
Institute for Plasma Research India[3)],
Research Institute for Applied Mechanics, Kyushu University [4)],
Interdisciplinary Graduate School of Engineering Science, Kyushu University [5)],
Graduate School of Engineering, Kyoto University [6)],
National Institute for Fusion Science[7)],
Plasma Research Center Univ. of Tsukuba[8)]
Department of General Education Kyushu Tokai University[9)]

e-mail contact of main author: zushi@triam.kyushu-u.ac.jp

1) On leave from Southwestern Institute of Physics, 610041, China
2) On leave from Institute for Plasma Research, India

Abstract. An overview of steady state tokamak (SST) studies on TRIAM-1M (R_0 =0.8 m, a×b=0.12 m×0.18 m and B =8T) is presented. Current ramp-up scenario without using centre solenoid coils is reinvestigated with respect to controllability of the current ramp-up rate at the medium density region of 1-2×10^{19} m^{-3}. The plasma is initiated by ECH (fundamental o-mode at 170GHz with 200 kW) at B=6.7 T and the ramp-up rate below the technical limit of 150 kA/s for ITER can be achieved by choosing LH power. The physics understanding for the enhanced current drive (ECD) mode around the threshold power level is progressed from a viewpoint of the transition probability. A transition frequency f_{trans} for the ECD transition is determined as a function of P_{CD}. At ~70 kW no transition occurs for f_{trans} of ~ 0.017Hz meaning almost zero transition probability. With increasing $P_{CD} > P_{th}$ f_{trans} increases up to 10 Hz and the transition tends to occur with high probability. The record value of the discharge duration is updated to 3h 10min in low $\bar{n}_e$ ~ 1× 10^{18} m^{-3} and low power (< 10 kW) discharge. The global particle balance in long duration discharges is investigated and the temporal change in wall pumping rate is determined. Although the density is low, at 30 min after the plasma initiation the gas supply was stopped to maintain the density constant. After that the density is sustained by the recycling flux alone until the end of the discharges. In addition to the recycling problem, in the high power and high density experiments, the localized PWI affects the SSO of the tokamak plasma. The effects of enhanced influx of metal impurities (Fe, Cr, Ni, Mo) on sustainment of the high performance ECD plasma are investigated. In order to evaluate the helium bombarding effects on the plasma facing component and hydrogen recycling in the future burning plasma, microscopic damage of metals exposed to long duration helium discharges was studied. The total exposure time is 128 sec. From thermal desorption experiments for the specimens the amount of retained helium was evaluated 3.9×10^{20} He/m^2 and the scale length of ~ 1mm in the SOL.

1. Introduction

TRIAM-1M (R_0 =0.8 m, a×b=0.12 m×0.18 m and B =8T) is a high toroidal magnetic field superconducting tokamak. Two kinds of lower hybrid current drive systems have been installed. One consists of a 2.45 GHz 50 kW cw kystron tube, oversized transmission waveguides, phase shifters, and a grill antenna with four waveguides. The launched peak refractive index $N_{||}$ is ~1.6. The others are two sets of cw 8.2 GHz system, whose power is 200

kW each and antenna is a grill with 2×8 waveguides. $N_{\|}$ can be varied from 1.6 to 2.5 during a single discharge for one system. They are located around the torus separating by 180°, but are operated by a single oscillator. During these years from the last IAEA Fusion Energy Conference [1] an ECRH system was installed. This consists of a gyrotron (200 kW and five seconds pulse width at 170 GHz), optical matching box, corrugated waveguides whose diameter is 61.5 mm, a differential pumping system keeping pressure below 10^{-5} torr in the waveguide system, and a single ended corrugated antenna whose diameter is 31.75 mm. Using a differential pumping system no vacuum window separating the waveguide system from the plasma vacuum chamber is used. The ECRH wave in the ordinary mode is injected perpendicularly to the toroidal magnetic field. In order to avoid the direct reflection from the opposite chamber wall, an inclined flat plate is installed behind the limiter surface.

The following experiments have been carried out to advance the SST concept [2,3]. First, establishment of the current ramp-up scenario and rf power controllability of ramp-up rate have been studied from a viewpoint of future tokamak without centre solenoid coils. In a superconducting tokamak device there is a technological limit for current ramp-up rate, for example, ~150 kA/s for ITER [4], which is restricted by applied voltage to the superconducting poloidal coils and AC loss in their coils. In addition to the technical problems, there is also a physical limit for non-inductive current ramp-up at the higher density, for example, rf turn-on time [5] or current turn-on time [6].

Second, physics understanding for the enhanced current drive (ECD) mode around the power threshold behaviour has been progressed. The ECD mode is characterized by simultaneous improvement of transport and current drive efficiency, and both improvements show a power hysteresis relation [1,3,7,8,9]. A physical meaning of the power hysteresis and also power threshold are investigated using an advantage of steady state operation. A transition frequency f_{trans} from a non-ECD plasma state to the ECD state is precisely determined under the condition of fixed LHCD power in time. The power dependence of f_{trans} is studied within a power hysteresis region (90~140kW). It is found that f_{trans} is blow 0.01Hz at P_{CD}~70 kW and there occurs no transition, but it increases non-linearly up to ~10 Hz with increasing P_{CD} to 140 kW and transition occurs easily. Thus, in a statistical sense with a help of f_{trans} the threshold power and probability for ECD transition can be explained in the hysteresis power region.

Third, two problems concerning with particle control affecting steady state operation have been studied. One is global particle balance including the wall pumping, wall saturation, wall fuelling, external pumping, and external fuelling [10,11,12]. In order to understand the gas release from the plasma facing components temperature and heat deposition measurements have been also done during the steady state discharge. The other is the impurity influx from plasma facing components composed of metallic materials (iron Fe, chromium Cr, and nickel Ni of the vacuum chamber, and molybdenum Mo of the limiter and divertor plates). The low Z material coating has never been done in TRIAM-1M. Since ultra long discharges have so far been obtained in the limiter configuration, the chamber wall is now covered with deposited molybdenum [14,15]. The spectroscopic measurement in the visible range shows that the metallic impurity influx from the localized region on the PFC plays an important role for a termination of the ECD mode.

Finally, the effects of hydrogen/helium bombardment on the material surface are investigated. This will be useful to evaluate the effects of helium produced via D-T nuclear reaction in the future burning plasma. It has been reported that hydrogen charge exchange neutrals play an essential role on radiation damage [16]. The minimum energy for damage of incident particles with mass M_1 to the target atom with mass M_2 can be estimated from the following equation.

$$E_{\min} > \frac{(M_1 + M_2)^2}{4M_1M_2} E_d ,$$

where M_1=1 for H or 4 for He, M_2 =96 for Mo, and E_d=35 eV for Mo. E_{min} is 850 eV for hydrogen atom and 228 eV for helium atom. Thus, the helium discharge experiment is conducted. Radiation damage is measured by TEM and the amount of the retained He are estimated by TDS.

2. Non-inductively current ramp-up and controllability of ramp-up rate

As mentioned in section 1, the non-inductive current ramp-up scenario and controllability of the current ramp-up rate are tested at the higher density regime, especially, the characteristic time constant for current ramp-up is studied. Although so far many current ramp-up experiments by non-inductive methods have been performed [19-21], relatively low density plasma (0.05~ 0.5×10^{19} m^{-3}) has been used, as shown in Fig.1. In ITER an ECRH initiated target plasma with higher density is thought in the non-inductive ramp–up scenario [4]. We investigated the similar situation on TRIAM-1M. A target plasma is initiated by ECH of 170GHz at B=6 - 6.7T. Then LHWs are injected to drive the plasma current. The target density $\bar{n}_e$ of 1-2×10^{19} m^{-3} is obtained under the conditions of ECRH of 70 – 150 kW and gas pressure from 1.2×10^{-6} torr to 2×10^{-5} torr. The electron temperature is not measured, but is deduced > 20-50 eV from spectroscopic OV (278 nm) measurement. The small current (≤ 2kA) flows in this ECRH plasma and its flow direction depends on the vertical field, which is similar to the previous results [17]. A vertically elongated plasma is initially observed at the major radius corresponding to the resonance magnetic field. The luminous points on the top and bottom portion of the poloidal limiter are also observed, indicating the toroidal drift of the plasma and resulting interaction between plasma and limiter. In order to find optimum conditions of ECH plasma from a viewpoints of ramp-up current B_t and equilibrium vertical field B_v are surveyed. The best condition was obtained at B_t=6.7T where ECW breakdown occurred by 4 cm from the plasma centre of R_p=0.84 m. This off-axis breakdown is necessary for the desirable coupling between the lower hybrid wave launcher and the scrape-off plasma. Since the initial density is high enough, the coupling efficiency is about 90 % even in the initial phase. The typical current ramp up result is shown in Fig.2. In the current ramp-up phase the waveform of I_p is well fitted by the following simple model, $I_p(t)=I_p^{ss}(1-\exp(-t/\tau_{rise}))$, where I_p^{ss} is a steady state value and τ_{rise} is a characteristic ramp-up time. In these experiments, for t < 0.1s, the pre- programmed vertical field B_v of ~ 60G is applied and I_p grows with shorter τ_{rise} of ~ 0.1s, and then for t > 0.1s the plasma position is controlled by a feedback loop and I_p increases with longer τ_{rise} of ~ 0.2s. A model to describe the two kind of τ_{rise} is discussed in detail [22]. In this model phase velocity of the injected LH waves is assumed to evolve exponentially with a time constant, which is different from L/R (inductance/ resistance) time constant. In figure 3 current ramp-up rate I_p^{ss}/τ_{rise} and τ_{rise} are plotted as a function of injected

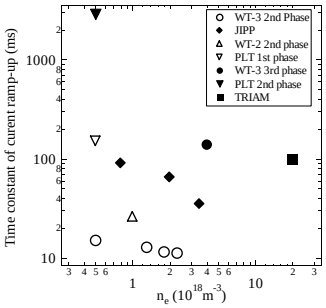

Fig. 1 The time constant of current ramp-up as the function of $\bar{n}_e$ in the ECRH + LHCD current start-up in various tokamaks[3-6].

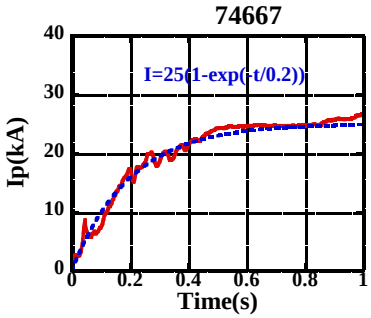

Fig.2 Current ramp-up and steady state sustainment of LHCD plasma is demonstrated without using centre solenoid coils. This discharge lasts for more than 30sec. A plasma is initiated by ECRH at B=6.7T Blue dotted line is a model curve $I_p(t)=I_p^{ss}(1-\exp(-t/\tau_{rise}))$, with I_p^{SS}=25 kA and τ_{rise}= 0.2 s.

power. Data are taken from current ramp-up experiments with I_p^{ss} > 20 kA and at least 2 sec duration (~10 times τ_{rise}), and also include discharges with ECD transition occurring at t=0.5 sec (~ 2 τ_{rise}). The current ramp-up rate I_p^{ss} /τ_{rise} seems to increase with increasing P_{CD} and can be controlled below the technical limit of ~ 150 kA/s in ITER when P_{CD} is below 100kW. The obtained τ_{rise} is 0.15-0.3 sec.

We will discuss the physical meaning of τ_{rise} and compare with the theoretical ramp-up time constants [5,6,19] in the more high density regime. First, τ_{rise} is compared with "RF turn-on time" $\tau^{rf}_{turn\text{-}on}$ [5], which has been well agreed in low density plasmas [19]. Observed τ_{rise} values, however, are higher than the calculated $\tau^{rf}_{turn\text{-}on}$ of 37-55 ms. In this calculation upper and lower parallel refractive indices $N_{||}$ are chosen 2.5 and 1.2, which are calculated at the waveguide phasing of 90°. The density is 1×10^{19} m^{-3} and T_e is assumed 20 – 100 eV. This theoretical value only describes development of the distribution function in velocity space. Since there is a very large spectrum gap between the injected wave phase velocity and thermal velocity of electrons, up-shift of the injected $N_{||}$ is required. According to the extended theory including the induced electric field [5,23,24], we will determine the actual value of $N_{||}$ contributing the ramp-up.

Second, the up-shifted $N_{||}^U$ and power absorption efficiency P_{abs} = $\eta_{abs}\times$ P_{CD} can be evaluated in terms of P_{el}/P_{abs} and v_{ph}/v_r, where P_{el} is the electric power flowing into magnetic field energy, v_{ph} is the phase velocity associated with $N_{||}^U$, v_r is the critical runaway velocity calculated from the induced electric field. Z_{eff} of 5 is assumed. For typical ramp-up experiment adjusting free parameters $N_{||}^U$ and η_{abs} are determined 6.0 and 0.2, respectively. If we substitute n_e of 1×10^{19} m^{-3} and $N_{||}^U$ of 6 into $\tau^{rf}_{turn\text{-}on}$, discrepancy becomes significant, because $\tau^{rf}_{turn\text{-}on}$ has following dependences of $n_e^{-1}T_e^{0.25}N_{||}^{-2.5}$. Although the ramp-up phase can be well fitted in low density plasma with initial decaying current in ref. [20, 24], a new theory taking into account the large spectral gap will be necessary for describing the dynamic process in the current ramp-up.

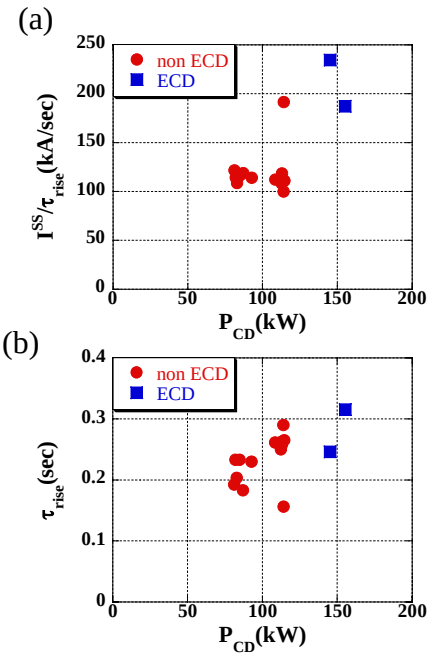

Fig.3 Current ramp-up rate (a) and ramp-up time (b) are plotted as a function of P_{CD}.

Third, it is pointed out in ref. [6] that plasma current ramp-up for non-inductive current drive is governed by $\eta(0)$ central resistivity, which introduces a natural timescale, $\tau_0=a^2\mu_0/\eta(0)$, for ramp-up. Here a is the minor radius and μ_0 is permeability in vacuum. In our condition τ_0 is 0.14 – 0.2 s evaluated by T_{e0}= 400-500eV measured at steady state, but it becomes much less than observed τ_{rise} if we use T_e of 20-100 eV expected in the early phase. Based on the simulations in ref. [6] the current ramp-up time is greater than or comparable to $\tau_0\times\Delta I/I_0$, where ΔI is the incremental increase in the plasma current and I_0 is the initial current. This natural time constant introduces the following simple equation governing the current ramp-up rate,

$$\frac{dI}{dt} = S_{CD} - \frac{I}{\tau},$$

where S_{CD} is the current source rate and τ is a time constant of current ramp-up. From this equation we can easily obtain the assumed model, $I_p(t)=I_p^{ss}(1-\exp(-t/\tau_{rise}))$, where $S_{CD}= I_p^{ss} /\tau_{rise}$. Obtaining a relation between τ_{rise} and $\tau_0\times\Delta I/I_0$ is left for future.

Finally, we will discuss about the controllability of the current ramp-up rate. In non-inductive current ramp-up scenario, we have to obtain the required I_p^{ss} and keep the ramp-up rate below the limit. Using current drive efficiency η_{CD} ($\equiv n_e I_p^{ss} R/P_{CD}$) and the empirical temperature scaling $\eta_{CD}=<\eta><T_e>$ [4], in order to get required I_p^{ss} it is necessary for both P_{CD} and $<T_e>$ to be increased for fixed n_e, R and $<\eta>$. Here $<T_e>$ is the volume averaged electron temperature. Using the natural time constant in order to keep the ramp-up rate below the limit, $P_{CD}/\sqrt{T_{e0}}$ should be kept below certain value for given $<T_e>$ and fixed temperature profile ($<T>$ is replaced by $T_{e0}\times$profile factor). Thus, the electron heating is favourable, but for given T_{e0}, P_{CD} is strictly limited. The electron temperature control during the ramp-up phase should be tested.

3. Transition frequency for the ECD transition in the power hysteresis region

The transition behaviour of the LHCD plasma to the ECD mode has been intensively studied at around the threshold power P_{th} at B=6.4-7 T. ECD is characterized by simultaneous enhancement of energy confinement and current drive efficiency $\eta_{CD}= \bar{n}_e I_{CD} R_0/P_{CD}$ [1,3,7,8,9]. Two typical transitions are shown in Fig. 4. The current drive power is raised from 100 kW (≥ threshold power) to 150 kW (> threshold power) for 2 sec from t=1.5 s to 3.5 s and total pulse width is 4.5 s. An ohmic target plasma is used, but 0.5 sec after OH breakdown plasma current is sustained by LHW alone. The density is ~1.3 $\times 10^{19}$ m^{-3} in the phase 1, and then increases by ~15 % when power is increased. At an arrow it increases further by ECD transition. In the phase 4 the ECD transition occurs again at lower power level. The former is a 'forced transition' by increased power and the latter is a 'self-transition' at the constant power. In fig. 5, time trajectories of a measure of the ion confinement time ($\tau_i^* = n_e T_i/P_{CD}$) and current drive efficiency are plotted as a function of power. A clear hysteresis curve is seen for the forced transition. At the same power of ~ 100kW the self-transition follows back the trace of the forced transition (denoted by green curve). This shows that there are two ways from the low state to the high state and vice versa at the same power, if the power is considered to be only the driving term in this system. Recent theory emphasizes that the transition process should be described statistically by a transition probability [25].

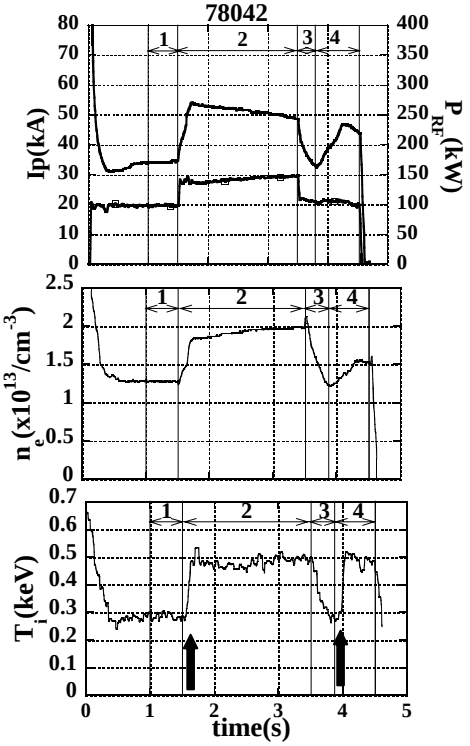

Fig.4 A typical discharge with two ECD transitions. Arrows indicate the ECD transition.

In order to study the statistical nature of ECD transition at around the threshold power, a measure of the transition frequency which is expected to be associated with the transition

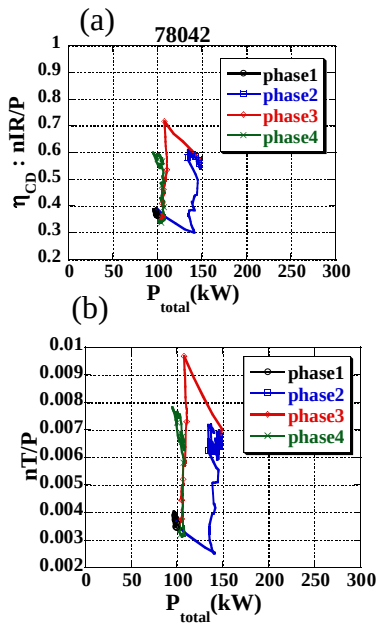

Fig. 5 Power hysteresis curves for current drive efficiency (a) and a measure of ion confinement time(b). Initial point is the left-bottom corner and time proceeds from left to right, from bottom to top, from right to left, and from top to bottom.

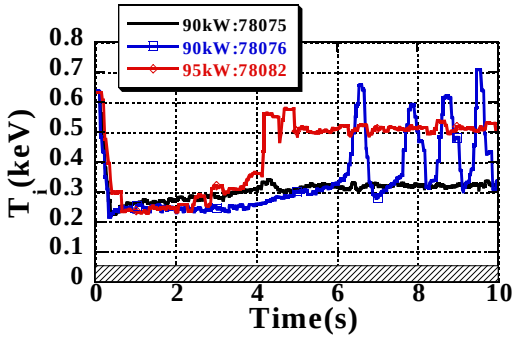

Fig. 6 ECD transition is demonstrated at P~P_{th}. With a long $\tau_{transition}$ ECD transition occurs at 4.2 s and high T_i is sustained for 16 s at P_{CD} ~95 kW in shot #78082. An oscillatory transition (#78076) and non-ECD are found at P_{CD}~90 kW.

probability is introduced, that is, a time $\tau_{transition}$ is defined as a time difference t_{ECD} - t_{rf} with which the transition occurs after the power is applied at $t=t_{rf}$.

Time evolution of T_i in three typical discharges at around P_{th} ~ 90 kW are shown in Fig6. Shot #78075 is a normal steady state discharge with power of 90 kW and T_i variation is less than a few % for 20 seconds (in figure the half of the discharge is only shown). An oscillatory improved plasma between ECD and non-ECD states at $\bar{n}_e$ ~1.2 ×10^{19} m^{-3} is shot #78076. T_i starts to increase with $\tau_{transition}$ of ~ 6 s and then it oscillates with a frequency of ~1.3 Hz which is given by the H_α feedback system for density control. In the third case the clear transition to the ECD mode with $\tau_{transition}$ of 3.8 s and its long sustainment is obtained in shot #78082 at 95 kW.

In figure 7 the transition frequency ($1/\tau_{transition}$) is plotted as a function of P_{CD} for various discharges with the longest duration up to 60 sec. At ~70 kW no transition occurs for at least 60 seconds discharge duration meaning almost zero transition probability. For non-ECD discharges the upper limit of $1/\tau_{transition}$ is only given. With increasing $P_{CD} > P_{th}$ the transition tends to occur with increasing high probability, that is, larger value of $1/\tau_{transition}$. The frequency increases logarithmically within the hysteresis power window (90-140 kW), as shown in Fig. 5. The spontaneous transition will occur with the frequency of inverse energy confinement time of 100-200Hz. This power level is the minimum power required to trigger the transition with high probability. On the other hand, the absolute power threshold with minimum probability is considered to be ~ 80 kW at which the transition frequency is ~ 0.1 Hz. At around

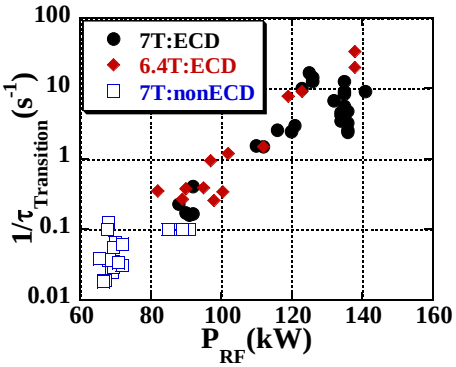

Fig.7 Transition probability (frequency) is plotted as a function of P_{CD}. Open squares correspond to non-ECD discharge with duration of ' $\tau_{transition}$'. At 70kW probability is zero for a 60 s discharge with no transition. At 80-90 kW the probability is marginal for ECD.

this power the transition probability is not only reduced, but also the steady state sustainment becomes difficult even if the transition would occurred, as shown in fig.6. Thus advantage of the steady state discharge is demonstrated even for 'transient events'.

4. Global particle balance and impurity problems in steady state plasma

The progress of the steady state tokamak operation in 2.45 GHz LHCD plasma is shown in Fig. 8 and the record value of the discharge duration of 3h 10min is achieved. Several aspects of these long pulse operation discharges are studied from a viewpoint of global particle balance including balance of wall pumping and fuelling, impurity influx and accumulation, and energy deposited on the plasma facing component [26]. In this low $\bar{n}_e \sim 1\times 10^{18}$ m^{-3} and low power (< 10 kW) discharge the fuelling was stopped at t~ 30min and after that $\bar{n}_e$ could be sustained without gas fuelling until the end. The temporal change in wall pumping rate was measured. The wall pumping rate of 2.4×10^{16} atoms /m^2/s is evaluated at t=10-20 min, but it becomes negative (-8×10^{15} atoms/m^2/s) for t> 30min. This means the wall acts as a particle fuelling source after the gas puffing was stopped. Fig. 9 shows the time evolution of the wall inventory. Light and heavy impurity influxes evaluated from visible spectroscopic measurements of oxygen II (465 nm) and molybdenum MoI (386 nm) were constant in time and no accumulation of oxygen (from OV 278 nm) and molybdenum (from Mo XIV 37 nm) were observed. However, H_α increased gradually by a factor of 1.6 with a time constant of ~ 50 min until the end of discharge. The limiter temperature is measured by an IRTV and it is observed that it saturates at 600-800 °C within t~5 min. This value is obtained with an assumption of the Mo emissivity of unity. The maximum wall temperature increases up to ~120 °C with a longer time constant of 10 to 30 min. This slower temperature rise might enhance gas release from the wall. The global energy deposition on limiters, wall, and divertor plates is also studied by thermistor measurement of cooling water temperature of the inlet and outlet water flow. Energy deposition is distributed in the following fraction: 67% on vacuum

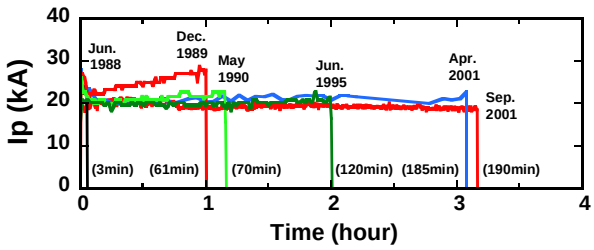

Fig.8 Progress of SST operation. 2.45GHz LHCD is used.

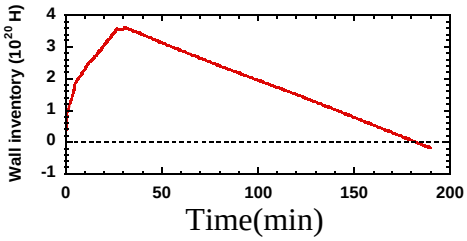

Fig. 9 Wall inventory in 3h 10min discharge.

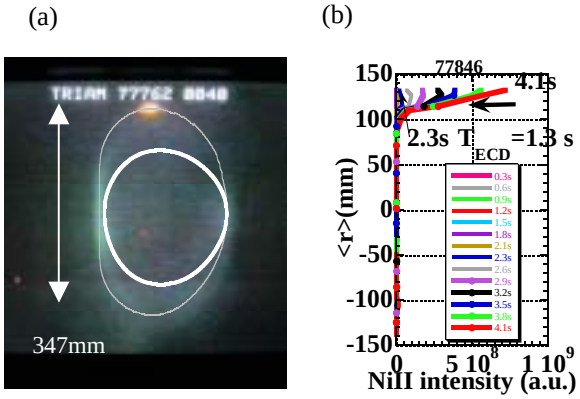

Fig.10 (a)Hot spot (bright portion on the top of the figure) in non-ECD mode. Thick curve is the last closed flux surface. The thin line indicates the limiter. (b) Temporal NiII intensity vertical profiles in ECD discharge occurred at T_{ECD}~1.3 s and Ni II intensity increases from 2.3s abruptly. Arrow indicates the limiter radius.

chamber wall, 10 % on divertor plates and 22% on limiters. Thus in order to sustain the long duration discharge the matter of the highest priority is the density control after the wall is saturated.

In addition to above recycling problems associated with the entire wall surface, the localized plasma-wall interaction is an obstacle to get a steady state high performance plasma. Especially this becomes problem in the higher power (> 70 kW) higher density (> 1×10^{19} m^{-3}) 8.2 LHCD plasma. Figure 10(a) shows a typical hot spot on the limiter (#1) in the non-ECD 60 sec discharge at ~ 70 kW. It appears at t ~ 30s. In case of $P_{CD} > P_{th}$ when the ECD transition occurs the hot spot appears at the same position 1s -2 s after the transition, but its brightness is enhanced. It is also found that Fe, Cr and Ni influx relevant to the hot spot from the topside (electron toroidal drift side) is significantly enhanced when ECD occurs, but oxygen flux does not. In the case of non-ECD discharge this kind of enhanced metal ion influx is not observed, although a similar hot spot is formed. Figure 10(b) shows the temporal vertical metal intensity profiles in the ECD phase (t > 1.3 s), where the LCFS radius is ~114mm. The intensity increases non-linearly in time. The scale length of intensity profile is ~17mm in the SOL and it increases in time from 3.9 mm to 7.4 mm inside the LCFS. They are roughly in the same order of the ionisation mean free path of 3~ 19 mm with assumptions of T_e=10-20 eV, $n_e=0.5\times 10^{19}$ m^{-3}, and the mean energy of evaporated metal ions. It should be noted that the intensity profile shows strong up-down asymmetry, which means the metal impurity influx origins from the localized portion of the top of the chamber. The evaporation rate, that is, metal atom influx non-linearly depends on the surface temperature and evaporation entropy [27]. The reason for such asymmetry heat load on the top portion of the torus is under study with respect to orbits of energetic electrons accelerated near the LH grill antenna [28,29], or ripple trapped loss of the energetic electrons with small $v_{||}$. In order to evaluate the lost energetic passing electrons a movable limiter equipped with a cooling water system is inserted on the equatorial plane along the major radius [22, 30]. The result shows the obtained heat load is within the plasma load in the SOL region, and there is no indication of the energetic passing electron loss. However, heat load of the chamber wall and limiter measured by thermistor show a clear change depending on non-ECD and ECD. The reduction of the limiter heat load is ~ 1-2 kW and increment of the chamber heat load is the same. We think that the maximum lost power via the conversion from the passing to the ripple trapped particles is ~ 1-2 kW on the localized part of the chamber wall. The heat flux is expected to be ~ 2-5 MW/m^2 with assumptions of each $1cm^2$ area times four portions. This heat flux leads to the wall temperature up to 1000-1600 K within 4 sec and metal influx due to evaporated atom is ~ 10^{16} $atoms/m^2s$.

In order to study how the metal influx affects the lifetime of the discharge, a time $\tau_{IP=90\%}$ for steady state operation of the ECD mode is in-

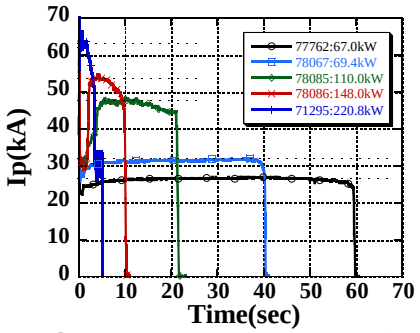

Fig. 11 Plasma current in non-ECD ($P<P_{th}$) and ECD transition plasma ($P>P_{th}$). $\tau_{0.9}$ is determined from these series.

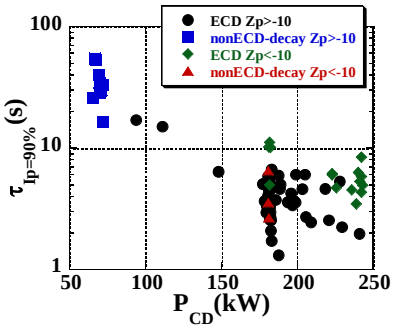

Fig. 12 $\tau_{IP=90\%}$ v.s. Power. $\tau_{IP=90\%}$ decays with P_{CD}. In order to reduce the PWI at the topside the plasma centre is moved downward by Zp. For Zp<-10 mm $\tau_{IP=90\%}$ is increased, although ECD transition is delayed further.

troduced, where $\tau_{IP=90\%}$ is defined as the time period for the plasma current to be sustained within 90% of the maximum value. Figure 11 shows the Ip evolution in ECD and non-ECD plasmas above and below P_{th}. Since no significant drop of Ip is observed in non-ECD discharges, $\tau_{IP=90\%}$ corresponds to the discharge pulse width. In the ECD discharge, however, Ip is increased at the transition and then is sustained for some time period, and finally it starts to decay quickly (see #78085,78086). The metal ion influx from the topside well correlates with this sequence. With increasing power the metal ion intensity enhances much and Ip drops drastically (see #71295). In Fig. 12 these results are summarized. The longest SSO period in ECD mode ($\tau_{IP=90\%}$ ~18 sec) is achieved at $P_{CD} \sim P_{th}$. With increasing power (>> P_{th}) it becomes difficult to enlarge $\tau_{IP=90\%}$. In order to increase it the plasma vertical position (Zp) is shifted downward. The $\tau_{IP=90\%}$ of ~ 10s at P_{CD}~2×P_{th} is succeeded at Zp~-18 mm, but the metal flux from the topside is not reduced much and the metal flux from the bottom side appears. Further optimisation for quenching the hot spot and minimizing the local PWI effects is left for SSO of high performance plasma.

5. Helium irradiation effects on the surface materials

High-energy charge exchange (CX) particles bombarding the plasma facing components may cause not only physical sputtering but also damage inside the materials due to its rather high energy [13-16,31]. We have shown that CX-hydrogen caused the microscopic radiation damage in metallic specimens exposed to the long duration discharge 2.45 GHz LHCD hydrogen plasmas [16]. The depth distribution of accumulated radiation damage (dislocation loops) shows a significant contribution of the high energy (several keV) CX neutrals. The minimum incident energy of bombarding hydrogen atom is ~ 850 eV for damage on the Mo specimen. Observed up-down asymmetry of the damage on the specimens viewing a plasma vertically indicates that the lower half of the plasma is the major source of energetic CX flux, and it can be interpreted by CX flux from the energetic ripple trapped particles drifting in the downward direction under this B_t condition. In the case of burning plasma, however, we should take into account the effects of helium because it is well known that helium atoms have much stronger effects on material damage than hydrogen atoms. Thus effects of helium ions and charge exchanged neutral helium ($He^+ + He^0 \Rightarrow He^0 + He^+$) on material damage were investigated in helium LHCD plasma at 8.2 GHz [32]. Typical discharge duration was ~ 7 s and the total exposure time was ~ 125 s (~18 shots). Experimental conditions are as follows; $\bar{n}_e \sim 1\times 10^{19}$ m^{-3}, Ip > 20 kA, $T_i(H)$ < 0.2 keV , P_{CD} ~ 150 kW and B=7 T. A typical discharge is shown in Fig. 12. Although the working gas is helium, this plasma is not a pure helium plasma and rather contaminated by hydrogen which is trapped in, released and recycled from the plasma facing materials. T_i is measured from the hydrogen CX energy spectrum. Since the

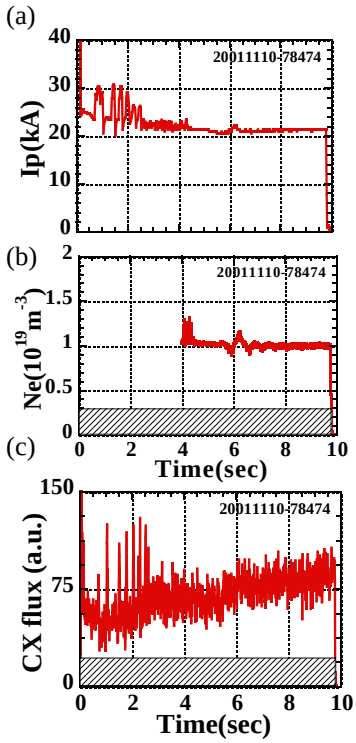

Fig.13 *A typical discharge of He plasma, Ip(a), n_e(b), and charge exchange flux at ~0.3 keV(c). 8.2 GHz LHCD(hatched area) is used at B=7T. The power is 150 kW.*

temperature equilibrium time is ~ 0.1 ms for He^{2+} and proton under this condition, ion temperature of He ions is considered to be the same as $T_i(H)$. Since the ion temperature is lower than those in ref. [16], relatively strong effects of helium compared with hydrogen is expected because E_{min} for incident helium atom is ~ 228 eV for Mo damage.

A water-cooled collector probe system has been installed on the TRIAM-1M, as shown in Fig.13. Three kinds of materials Mo, W, and bulk copper were attached on the head. Pre-thinned vacuum-annealed molybdenum and tungsten disks of 3 mm^{ϕ} were used for the damage analysis and bulk copper plates for the detection of implanted helium. The probe head was inserted in the SOL through a horizontal port; 11 mm behind the poloidal limiter (#9) surface. The location of the limiter is the right hand side with respect to the probe. The temperature of the probe head during discharges was almost constant at 24°C.

In order to collimate the particle incident directions and to avoid the effects of charged particles, the probe-specimens were placed in the deep holes at the plasma facing side (P-side). Each hole directs to different directions from the bottom to the top and from the left to the right of the plasma with semiangle of 14 degrees. Some specimens were directly mounted on the surface of P-side and the electron drift side (E-side) of the probe head.

After the discharge experiments, transmission electron microscopy TEM and thermal desorption spectroscopy TDS have been done. The microstructure of the pre-thinned molybdenum specimens directly placed on the probe surface at P-side was observed by means of TEM. Considerably large amount of dislocation loops (black images in Fig. 15(a)) and very dense fine bubbles (white image in Fig. 15(b)) were formed. Such heavy damage has not been observed in hydrogen plasma discharge experiments more than one hour. For Mo specimens placed inside the hole only dis-

(a)

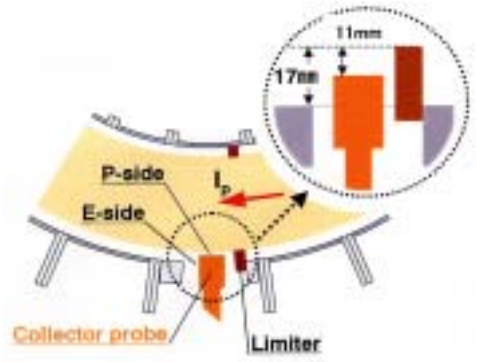

(b)

Fig.14 A schematic view of the collector probe system (a) and the probe head (b).

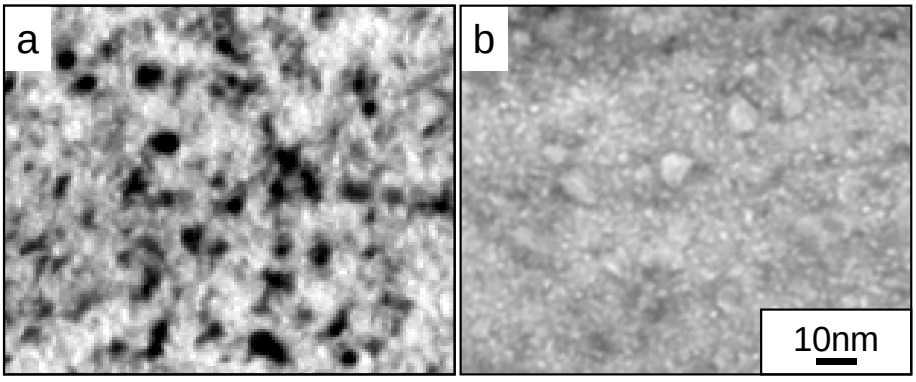

Fig.15. TEM image of radiation damage in molybdenum placed on the surface at the P-side. (a) image at small s condition. (b) image at large s condition

location loops were formed because the fluence is much smaller than that for the directly placed ones due to smaller solid angle opened to the plasma. By TDS (from room temperature to 1100 K) of the P-side bulk copper plates the amount of retained helium was estimated to be 3.9×10^{20}He/m^2. From the fluence dependence of the total retention of He the incident fluence is considered to be 6.1×10^{20}He/m^2. This means that the average flux of the helium at the plasma facing surface is at least $3.1\text{x}10^{18}$He/m^{2}s. A clear deposition of Mo on the E-side bulk copper specimens (< 16 mm from the limiter surface) was observed. TDS results for the specimens on the E-side show that the retention of He is > 10^{21}He/m^2. This value indicates that the He trapping site is formed by Mo deposition. The hydrogen recycling study in steady state operation under these circumstances is left as an urgent subject in near future.

Summary

Experimental results of SSO of LHCD plasma in TRIAM-1M are presented. Current ramp-up scenario without using centre solenoid coils is studied using ECH initiated plasma with respect to controllability of the current ramp –up rate. The ramp-up rate below the technical limit of 150 kA/s for ITER can be achieved by choosing LH power. The ramp-up time is compared with rf turn-on time or central resistivity time and it is found that obtained the ramp-up time is longer than the theoretical ones.

The statistical nature of the ECD mode is studied around the threshold power level. The transition frequency for ECD transition is introduced and is determined as a function of P_{CD}. At ~70 kW no transition occurs for more than 60 seconds duration meaning almost zero transition probability. With increasing $P_{CD} > P_{th}$ the transition tends to occur with high probability.

The record value of the discharge duration is updated to 3h 10min in low $\bar{n}_e \sim 1\times 10^{18}$ m^{-3} and low power (< 10 kW) discharge. The global particle balance including wall effects in long duration discharges is investigated. In addition to this recycling problem, in the high power and high density experiments, it is pointed out that the local PWI strongly affects the lifetime of the high performance plasma. Especially, it is found that power dependent local metal impurity influx from the hot spot terminates the high performance ECD plasma.

In order to evaluate the helium bombarding effects on the plasma facing component and hydrogen recycling in the future burning plasma, microscopic damage of metals and He retention are studied for specimens exposed to helium discharge of ~125 s. Large amount of dislocation loops and dense fine bubbles are observed by means of TEM. From TDS for the specimens the amount of retained helium is evaluated 3.9×10^{20} He/m^2.

References

[1] ZUSHI, H, et al., Nuclear Fusion **40** (2000) 1955.
[2] ITOH, S., et al., Nucl. Fusion **39** (1999) 1257.
[3] ZUSHI, H., et al., Nucl. Fusion **41** (2001) 1483.
[4] ITER Physics Basis, Nucl. Fusion **39** (1999) 2137-2664.
[5] FISCH, N.J., Rev. Mod., Phys., **59** (1987) 175.
[6] JARDIN, S.C., Nucl. Fusion **40** (2000) 1101
[7] ZUSHI,H., et al., J. Plasma and Fusion Research SERIES, Vol.3 (2000) 16-21.
[8] HANADA, K., et al Nucl. Fusion **41** (2001) 1539.
[9] HANADA, K., et al., J. Plasma and Fusion Research **77** (2001) 294-299.
[10] SAKAMOTO, M., et al., Controlled Fusion and Plasma Physics (Proc. 24th Eur. Conf. Berchtesgaden, 1997) Vol. 21A, partII (Geneva: European Physical Society) p 721.
[11] SAKAMOTO, M., et al., J. Plasma and Fusion Research **78** (2002) 52-58.
[12] SAKAMOTO, M., et al., Nucl. Fusion **42** (2002) 165-168.
[13] HIRAI, T., et al., J. Nucl. Mater. **258-263** (1998) 1060.

[14] HIRAI, T., et al., J. Nucl. Mater. **283-287** (2000) 1177-1181.
[15] HIRAI, T., et al., J. Plasma and Fusion Research SERIES, Vol.3 (2000) 284-287.
[16] HIRAI, T., et al., J. Nucl. Mater. **290-293** (2001) 94-98.
[17] TANAKA, S., et al., Nucl. Fusion **33** (1993) 505.
[18] KUBO, S. et al.,Phys. Rev. Lett.,**50** (1983) 1994.
[19] TOI, K., et al., Phys. Rev. Lett.,**52** (1984) 2144.
[20] JOBES, F., et al., Phys. Rev. Lett.,**52** (1984) 1005.
[21] JOBES, F.C., et al., Phys. Rev. Lett.,**55** (1985) 1295.
[22] HANADA, K.,et al., this conference 'Current ramp-up experiments in full current drive plasmas on TRIAM-1M'
[23] FISCH, N. J., KARNEY, C. F. F., Phys. Rev. Lett.,**54** (1985) 897.
[24] KARNEY, C. F. F., FISCH, N. J., JOBES, F. C., Phys. Rev. A **32** (1985) 2554.
[25] ITOH, S. I., ITOH, K., J. Phys. Soc. Jpn. **68** (1999) 1891, **68**(1999) 2611, **69**(2000) 408, **69**(2000) 427, **69**(2000) 3253,
[26] SAKAMOTO, M., et al., this conference,'Wall recycling expriments on TRIAM-1M'
[27] BEHRISH, R., J. Nucl. Materials **93&94** (1980) 498.
[28] GONICHE, M., et al., Nucl. Fusion **38** (1998) 919.
[29] RANTAMAKI, K. M., et al., Nucl. Fusion **40** (2000) 1477.
[30] HANADA, K., et al., 29th European Physical Society Conference on Plasma Physics and Controlled Fusion P-2.085, 'Measurement of prompt loss of energetic electrons in a long LHCD discharge on TRIAM-1M'
[31] FEDERICI, G., et al., Nucl. Fusion **41** (2001) 1295-2138.
[32] YOSHIDA, N., et al., this conference 'Microscopic Damage of Metals Exposed to the Helium Discharges in TRIAM-1M Tokamak and its Impact on Hydrogen Recycling Process'.